CHAPTER 3

Use of the Average Solvent Potential Approach in the Study of Solvent Effects

Ignacio Fdez. Galván[a], **Aurora Muñoz-Losa**[a], **Catalina Soriano-Correa**[b], **M. Luz Sánchez**[a], **M. Elena Martín**[a] and **Manuel A. Aguilar**[a]

Contents

[a] Área de Química Física, Universidad de Extremadura, Avda. de Elvas s/n, 06071 Badajoz, Spain
[b] Laboratorio de Química Computacional. FES-Zaragoza, Universidad Nacional Autónoma de México, 09230 Iztapalapa, México D.F., Mexico

Advances in Quantum Chemistry, Vol. 59
ISSN: 0065-3276, DOI: 10.1016/S0065-3276(10)59003-8

1. INTRODUCTION

In the last decades the search for environmentally friendlier solvents [1] has been accompanied on the theoretical side by a renewed interest in the development of methods oriented to understanding and predicting how the structure, properties, and reactivity of molecules are affected by the presence of a surrounding medium [2], with the hope that this knowledge will serve as a guide in the development of new solvents. In contrast to the pioneering works of Born [3], Kirkwood [4], Onsager [5], and so on, which were based on a classical description of the solute, the new methods use quantum mechanics (QM), which permits a more detailed description of the changes that the solute molecule suffers during the solvation process. The high level of calculation and accuracy that has been achieved in the quantum description of molecules and processes in vacuo is widely known; consequently, an additional objective of current solvent theories is to achieve a similar level for molecules and processes in solution. From a practical point of view, the ultimate goal is to have available effective methods that permit to calculate the geometry and energy of minima, saddle points, conical intersections (CIs), and so on, of molecules in solution and that include the contribution of dynamical electron correlation or the possible multiconfigurational character of the solute wave function.

The medium that surrounds the solute can be of diverse natures: a solid, a liquid, a glassy solid, a liquid drop, a membrane, or even an enzyme; however, the vast majority of biological or chemical transformations takes place in the presence of a solvent. Because of this, most of the examples presented here are referred to systems and processes in the presence of a liquid solvent, even if many of the ideas developed could be easily applied to other media.

The solvent can have very different effects on the solute molecules [6], it can modify the frequency and intensity of the solute spectral bands, the thermodynamics and kinetics of chemical reactions, the strength of molecular interactions or the fate of solute excited states. A change of solvent can drastically alter the behavior of a chemical system, and the choice of a proper solvent is one of the first decisions that a chemist must take when facing a spectroscopic, kinetic, or thermodynamic problem. For all these reasons, it is very interesting to have theoretical methods that can guide chemists in their choices. Unfortunately, the theoretical study of solvent effects is quite complicated, since the presence of the solvent introduces additional difficulties with respect to the study of analogous problems in gas phase. Among these difficulties, we can remark the following:

(1) Firstly, the great number of molecules involved in the description of bulk solvent polarization effects. Molecules placed at long distances have a nonnegligible effect on the solute properties. In general, in the

study of solvent effects, and depending on the type of solute–solvent interactions involved, it is necessary to include several solvent shells in the calculations.

(2) Secondly, the possible presence of specific interactions, mainly hydrogen bonds (HBs), between the solute and the solvent molecules located in the first solvation shell. The correct description of these interactions makes the use of microscopic solvent models compulsory.

(3) Finally, in solution there are a great number of solute–solvent configurations that are thermally accessible. Different solute molecules will have different environments and, consequently, slightly different properties. To obtain statistically significant results, it is necessary to include hundreds or thousands of solute–solvent configurations.

An additional complication comes from the fact that, in solution, the relevant energy to consider is the free energy and we must hence have at our disposal methods that permit the calculation of this quantity in an effective and computationally feasible way.

All these complications, large number of solvent molecules, possible existence of specific interactions, great number of solvent configurations, the necessity of determining free energy differences, and so on, have as a consequence a very large computational cost associated to the calculation of solvent effects. Along the years, researchers have developed different strategies to reduce the computational cost while trying to keep the accuracy of the calculations at an acceptable level. One of the most successful strategies has been the introduction of the mean field approximation (MFA) [7,8] that permits to replace the configurational average of a given solute property with the value obtained for this property when the solute is affected by an average solvent perturbation. In the next sections, we treat different aspects of the practical implementation of the MFA, paying especial attention to a method developed in our laboratory and that combines the MFA with molecular dynamics (MD) simulations.

2. THE MEAN FIELD APPROXIMATION

Whereas the increase of computational power in the last decades has permitted to tackle the study of certain solvent effects using a brute force strategy, as in ab initio dynamics, its application to most chemical and biological problems is far from being routine. In ab initio dynamics [9], one combines the quantum mechanical description of both the solute and the solvent electron distributions with the classical or quantum description of the nuclei movements. Consequently, it becomes necessary to solve the Schrödinger equation of several hundreds of molecules for several thousands of configurations. The computational cost of this strategy is so

high that in almost all the studies performed to date, it has been compulsory to reduce the description level of the wave functions, the number of molecules, or the number of solvent configurations.

In the search for theoretical methods that facilitate the study of solvent effects, two main strategies have been followed:

(1) Focused methods. The computational cost associated to the large number of solvent molecules can be reduced using focused methods; here, we center our attention on a small part of the system, in general, the solute or the solute and a reduced number of solvent molecules, which is described using high-level quantum mechanical methods. The description of the rest of the system, generally the solvent, is simplified using for instance dielectric continuum models, Langevin dipoles, molecular mechanics (MM) force fields, or a combination of them. Focused methods are valid when there is a clear separation between the solute and solvent wave functions and they fail when charge transfer between the solute and the solvent is not negligible. In this case, the solvent molecules closer to the solute should be included in the quantum part.
(2) MFA. The computational cost associated to the large number of thermally accessible solvent configurations, and hence of quantum calculations to perform, can be reduced using the MFA. In this approximation, one does not consider the effect of specific configurations, instead, the solvent perturbation enters into the solute molecular Hamiltonian in an averaged way.

These two approximations can be used independently or jointly. Thus, QM/MM [10] or ONIOM-type methods [11] are examples of focused methods, whereas dielectric continuum [12–14], reference interaction site model (RISM)–self-consistent field (SCF) [15–17], or averaged solvent electrostatic potential (ASEP)/MD [18–21] methods use simultaneously both strategies. To our knowledge there are no methods that use exclusively the MFA.

A measure of the success of the MFA is the great number of solvent theories where it is explicitly or implicitly used. Table 3.1 displays a classification of some solvent theories where this approximation is applied. The various theories differ in the description of the solvent. Thus, if the solvent is described as a dielectric, we get different continuum theories. They can, in turn, be classified according to the representation of the solvent perturbation: monocentric multipole [14], multicentric monopole [13,22,23], effective charges [12,24], and so on. Other descriptions of the solvent are also possible: as a conductor [25,26], using Langevin dipoles [27], or MM force fields. In the latter case, the solvent structure can be obtained using RISM theory [15–17], MD [18–21,28,29], or Monte Carlo simulations [30]. In the model proposed in our laboratory, named ASEP/MD, the solvent

Table 3.1 Classification of some of the most commonly used solvent theories that use the mean field approximation

	Conductor	Dielectric	Langevin dipoles	Molecular mechanics	
				RISM	MD
Monopole multicentric		SMx		RISM–SCF	
Multipole monocentric		Rivail, Mikkelsen			
No multipole	COSMO	PCM	Warshel	3D-RISM–SCF	ASEP/MD

structure is obtained from MD simulations and the solvent perturbation is described using potential fitted charges.

The great advantage of the MFA, and what partly explains its success, is that it permits to reduce the number of quantum calculations from several thousands to a single quantum calculation. The price that one must pay is the complete neglect of the correlation energy associated with the response of the solute charge distribution to the instantaneous changes in the solvent structure as a consequence of thermal agitation. Obviously, the MFA will be valid only if the contribution of this energy, known as Stark component [31,32], to the total solute–solvent interaction energy remains negligible. It has been shown, both theoretically [20] and experimentally [33], that this is usually the case. A recent study [34] of the errors introduced by the MFA in the calculation of free energy profiles of S_N2 Menshutkin reactions has concluded that these are lower than 0.5 kcal/mol.

3. THE ASEP/MD METHOD

Any theoretical method devoted to the study of solvent effects and intending to be of application to chemical problems of general interest must provide solution to, at least, the following problems: (1) the description of the mutual polarization of the solute and the solvent, (2) the location of critical points on free energy surfaces, and (3) the calculation of free energy differences between different solute–solvent geometries. In the following, we will show how ASEP/MD solves each one of these problems.

3.1. The mutual solute–solvent polarization

The ASEP/MD method is a focused method that makes use of the MFA. Since the solute is described quantum mechanically and the solvent by using MM force fields, it could also be classified into the QM/MM methods, more specifically, as a sequential QM/MM method [35] where QM and MD calculations are performed alternately and not simultaneously. As usual in focused methods [24], the ASEP/MD Hamiltonian is partitioned into three terms

$$\hat{H} = \hat{H}_{\mathrm{QM}} + \hat{H}_{\mathrm{class}} + \hat{H}_{\mathrm{int}}, \tag{1}$$

corresponding to the quantum part, $\hat{H}_{\mathrm{QM}}$, the classical part, $\hat{H}_{\mathrm{class}}$, and the interaction between them, $\hat{H}_{\mathrm{int}}$.

The energy and the wave function of the solvated solute molecule are obtained by solving the effective Schrödinger equation:

$$\left(\hat{H}_{\mathrm{QM}} + \hat{H}_{\mathrm{int}}\right) |\Psi\rangle = E|\Psi\rangle. \tag{2}$$

In general, in QM/MM methods this equation is solved for each solute–solvent configuration, which means several hundreds or thousands of times. The final value of the energy (or any other property) is calculated by averaging over all considered configurations.

From a computational point of view, it is convenient to split the interaction term into two components associated to the electrostatic and van der Waals contributions:

$$\hat{H}_{\mathrm{int}} = \hat{H}_{\mathrm{int}}^{\mathrm{elect}} + \hat{H}_{\mathrm{int}}^{\mathrm{vdw}}. \tag{3}$$

In many cases, it is supposed that $\hat{H}_{\mathrm{int}}^{\mathrm{vdw}}$ has little effect on the solute wave function and therefore it is usual to represent it through a classical potential that depends only on the solute–solvent nuclear coordinates. Obviously, it will contribute to the final value of the energy, and energy derivatives.

In this point the MFA is introduced. So, we define the MFA electrostatic interaction term, $\left\langle \hat{H}_{\mathrm{int}}^{\mathrm{elect}} \right\rangle$, as follows [7,8,18]:

$$\left\langle \hat{H}_{\mathrm{int}}^{\mathrm{elect}} \right\rangle = \int dr \cdot \hat{\rho} \cdot \langle V_S(r) \rangle, \tag{4}$$

where $\hat{\rho}$ is the solute charge density operator, and $\langle V_S(r) \rangle$, named ASEP, is the average electrostatic potential generated by the solvent at the position r. The brackets denote a statistical average over configurations in equilibrium.

The MFA energy is obtained by solving the following equation:

$$\left(\hat{H}_{\mathrm{QM}} + \langle \hat{H}_{\mathrm{int}} \rangle\right) |\Psi\rangle = \bar{E}|\Psi\rangle. \tag{5}$$

Note, that in the MFA we replace the average value of the energies obtained from Eq. (2) with the energy obtained in presence of the average solvent perturbation, that is, $\langle E \rangle \approx \overline{E}$.

Different solvation methods can be obtained depending on the way the term $\langle V_S(r) \rangle$ is calculated. For instance, in dielectric continuum models $\langle V_S(r) \rangle$ is a function of the solvent dielectric constant and of the geometric parameters that define the molecular cavity where the solute molecule is placed [12]. In ASEP/MD, the information necessary to calculate $\langle V_S(r) \rangle$ is obtained from MD simulations. In this way, $\langle V_S(r) \rangle$ incorporates information about the microscopic structure of the solvent around the solute, furthermore, specific solute–solvent interactions can be properly accounted for.

The basic scheme of the ASEP/MD method is very simple, see Figure 3.1. One begins by performing a quantum calculation of the solute molecule in gas phase. From this one can obtain the solute charge distribution that is introduced as input into an MD simulation. The rest of the simulation parameters can be obtained from suitable force fields. From the MD calculation, one gets the solvent structure, which permits to calculate the ASEP by averaging over the solvent configurations, the ASEP is then introduced into the solute molecular Hamiltonian. By solving the associated Schrödinger equation (5), we get the solute wave function but now perturbed by the solvent. The new solute charge distribution is again introduced into another MD simulation. The procedure is repeated until convergence is attained,

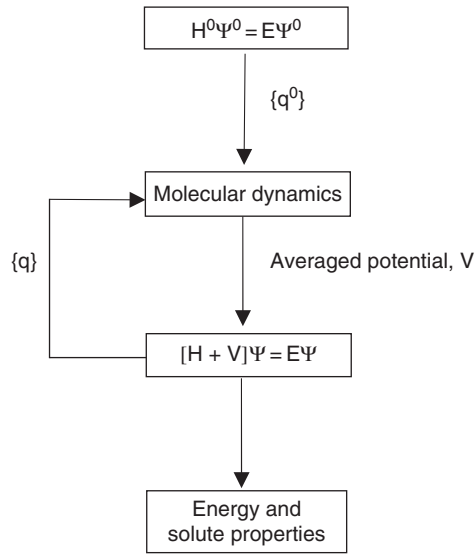

Figure 3.1 Flow chart of the ASEP/MD method.

something that occurs in a few cycles (less than ten, in general). Given that in our method quantum calculations and MD simulations are not simultaneous, there is a certain freedom to decide which configurations to include in the calculation of the ASEP. So, to decrease the statistical correlation between the selected configurations, we include only configurations separated by 0.05 ps or more. It is also important to remember that only the electrostatic term enters into the electron Hamiltonian.

The information that we get at the end of the ASEP/MD cycle is the energy, geometry, and wave function of the solute molecule polarized by the solvent and the solvent structure around it. Figure 3.2 displays how the solute charge distribution, which is represented by its dipole moment, and the solvent structure become mutually equilibrated during the ASEP/MD procedure. At the same time, the free energy of the system decreases until the system reaches the equilibrium and then it begins to fluctuate. The size of the fluctuations is a consequence of the finite size of the simulations.

One important point to clarify is the way in which the ASEP is calculated and introduced into the solute molecular Hamiltonian. We have checked several possibilities. The electrostatic solvent perturbation can be described through multipole expansions or using a set of point charges. In this last case, the charges can be determined in several ways. In general, especially when solute–solvent HBs are present, a representation using point charges is more adequate because the use of multipole expansions can introduce appreciable errors in the solute–solvent interaction energy. The simplest way to get the charges is to use for them the same values and positions used during the MD and then to divide the value of each charge by the number of solvent configurations included in the ASEP. The problem then is that the number of charges increases very quickly as the number of solvent molecules or system configurations gets higher. This approximation has been used, for instance, by Coutinho et al. [36]. To keep the number of charges tractable, we follow a somewhat more elaborated procedure: we consider explicitly only those charges associated to molecules that belong to the first solvation shell, the effect of the remaining solvent molecules is described by using potential-fitted charges.

The set of charges $\{q_i\}$ is obtained in three steps. The details are as follows [21]:

(1) Each selected configuration is translated and rotated in such a way that all of the solvent coordinates can be referred to a reference system centered on the center of mass of the solute with the coordinate axes parallel to its principal axes of inertia. This procedure is needed to get all the charges' coordinates referring to the same coordinate system.
(2) Next, one explicitly includes in the ASEP the charges belonging to solvent molecules that, in any of the MD configurations selected, lie inside a sphere of a given radius and that includes at least the first

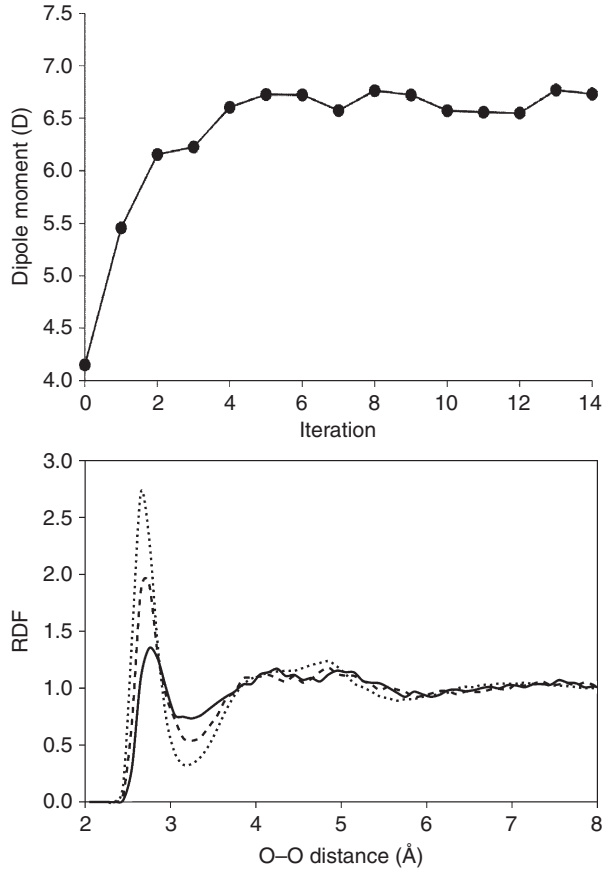

Figure 3.2 Mutual equilibration of solute and solvent during an ASEP calculation of formamide in water. Top: evolution of the solute dipole moment. Bottom: O—O RDF after the 1st (solid), 2nd (dashed), and 10th (dotted) iteration.

solvation shell. The value of every charge is then divided by the number of solvent configurations included in the determination of the ASEP. Next, to reduce the number of charges, one adds together all the charges lying less than a certain distance from each other, this distance is generally taken as 0.5 a_0.

(3) Finally, one includes a second set of charges representing the effect of the solvent molecules lying outside the first solvation shell. These charges are obtained by a least squares fit to the values of the ASEP originated by the outer solvent molecules in a three-dimensional grid

defined inside the volume occupied by the solute molecule. The solute volume is defined through a set of interlocking spheres of radius $f{\cdot}R_{\mathrm{vdw}}$, where f is a numerical factor close to one, and R_{vdw} are the Bondi radii of the solute atoms. These charges are obtained in such a way that they reproduce the electrostatic potential generated by the outer solvent molecules in the volume occupied by the solute.

The total number of charges introduced into the perturbation Hamiltonian varies generally between 25 000 and 35 000 depending on the size of the system.

3.2. Location of critical points on free energy surfaces

ASEP/MD uses a variant of the free energy gradient method [37–40] for the calculation of the gradients that drive the optimization process. In this method, the average force, $\langle F \rangle$, and Hessian, $\langle G \rangle$, felt by the solute atoms are used to optimize the geometry. The average force is defined as the derivative of the free energy (with a minus sign), and can be calculated as the average value of the potential energy derivative. The average Hessian takes a more complicated form, see below. In the original proposal of Okuyama-Yoshida et al. [37], these average values were obtained from QM/MM calculations where the solute molecule had a fixed geometry. The main advantage of this method is that it permits to obtain both stable and transition states. The main drawback is that the computational cost of calculating $\langle F \rangle$ and $\langle G \rangle$ is usually high. However, as we will show below, it is possible to reduce this cost by using again the MFA in the calculation of the gradient and Hessian.

The basis of the free energy gradient method is the following: Let $G = -kT \ln Z_{\mathrm{NVT}}$ be the Helmholtz free energy of a system formed by one solute molecule and N–1 solvent molecules and Z_{NVT} the quasi-classical canonical partition function. The force on the free energy surface (the force felt by the solute molecule) is

$$\langle F(R) \rangle = -\frac{\partial G(R)}{\partial R} = -\left\langle \frac{\partial E}{\partial R} \right\rangle = -\left\langle \frac{\partial E_{\mathrm{QM}}}{\partial R} \right\rangle - \left\langle \frac{\partial E_{\mathrm{int}}}{\partial R} \right\rangle, \tag{6}$$

R being the nuclear coordinates of the solute, E the energy obtained as the solution of the Schrödinger equation (2), and where we have assumed that E_{class} does not explicitly depend on the solute nuclear coordinates R. As before, the brackets denote a configurational average. Note that E incorporates both intra-, E_{QM}, and intermolecular, E_{int}, contributions.

In the same way the Hessian reads

$$\begin{aligned}\langle G(R,R')\rangle &= \left\langle \frac{\partial^2 E}{\partial R \partial R'} \right\rangle - \beta \left\langle \frac{\partial E}{\partial R}\frac{\partial E^{\mathrm{t}}}{\partial R'} \right\rangle + \beta \left\langle \frac{\partial E}{\partial R} \right\rangle \left\langle \frac{\partial E}{\partial R} \right\rangle^{\mathrm{t}} \\ &= \left\langle \frac{\partial^2 E}{\partial R \partial R'} \right\rangle - \beta \left[\langle F^2 \rangle - \beta \langle F \rangle^2 \right],\end{aligned} \tag{7}$$

where the superscript t denotes the transposition and $\beta = 1/kT$. The last term in Eq. (7) is related to the thermal fluctuations of the force.

As for the energy, it is convenient to split the interaction term into two components associated to the electrostatic and van der Waals contributions:

$$\langle F(R)\rangle = -\left\langle \frac{\partial E_{QM}}{\partial R} \right\rangle - \left\langle \frac{\partial E_{\mathrm{int}}^{\mathrm{elect}}}{\partial R} \right\rangle - \left\langle \frac{\partial E_{\mathrm{int}}^{\mathrm{vdw}}}{\partial R} \right\rangle. \tag{8}$$

Next, we use the MFA to simplify the gradient and Hessian expressions. Given that our final aim is to reduce the number of quantum calculations, this approximation is used for the two first terms of the R.H.S. of Eq. (8), but not for the van der Waals term that does not depend on the electron coordinates. Thus, we replace the configurational average of the derivatives with the derivative of the MFA energies obtained with Eq. (5), furthermore we neglect the force fluctuation term in Eq. (7) (since the Hessian is used only to accelerate the optimization procedure, this approximation has no effect on the optimized geometries but it can affect the harmonic frequencies evaluation). The validity of these approximations has been checked elsewhere [41]. The force now reads as follows:

$$\langle F(R)\rangle = -\frac{\partial \bar{E}_{\mathrm{QM}}}{\partial R} - \frac{\partial \bar{E}_{\mathrm{int}}^{\mathrm{elect}}}{\partial R} - \left\langle \frac{\partial E_{\mathrm{int}}^{\mathrm{vdw}}}{\partial R} \right\rangle, \tag{9}$$

with an analogous expression for the Hessian:

$$\langle G(R,R')\rangle = -\frac{\partial^2 \bar{E}_{\mathrm{QM}}}{\partial R \partial R'} - \frac{\partial^2 \bar{E}_{\mathrm{int}}^{\mathrm{elect}}}{\partial R \partial R'} - \left\langle \frac{\partial^2 E_{\mathrm{int}}^{\mathrm{vdw}}}{\partial R \partial R'} \right\rangle. \tag{10}$$

The advantages of the introduction of the MFA in the calculation of gradients and Hessians are evident, it permits to reduce the computational cost of these quantities in solution; in fact, the cost is similar to that of an isolated molecule.

3.3. Calculation of free energy differences

For most practical applications, one is interested in the free energy (FE) difference between different structures, states, or species, such as the ground and excited state in a photophysical process, and reactants, products, and transition state in a chemical reaction. Within the ASEP/MD methodology, the free energy difference in solution between two given states is approximated as follows [42]:

$$\Delta G_s = \Delta E_{\text{solute}} + \Delta G_{\text{int}} + \Delta ZPE_{\text{solute}}, \tag{11}$$

where ΔE_{solute} is the internal energy difference between the two solute states at QM level, ΔG_{int} is the difference in the solute–solvent interaction free energy, and $\Delta ZPE_{\text{solute}}$ includes the difference in zero-point energy as well as entropy and thermal contributions to the solute QM free energy. Although formally this equation takes the same form as in the QM-FE approach of Jorgensen [43], the meaning of the ΔE term is different. First, because the geometry of the two species involved are optimized in solution. Second, because the internal energy and charge distribution of the solute are determined in the presence of the solvent.

In Eq. (11), the internal energy difference between the two QM states is defined as

$$\Delta E_{\text{solute}} = E_{\text{B}} - E_{\text{A}} = \left\langle \Psi_{\text{B}} | \hat{H}^0_{\text{B}} | \Psi_{\text{B}} \right\rangle - \left\langle \Psi_{\text{A}} | \hat{H}^0_{\text{A}} | \Psi_{\text{A}} \right\rangle, \tag{12}$$

where, $\hat{H}^0_{\text{X}}$ is the in vacuo Hamiltonian for the state X, and Ψ_{X} is the electronic wave function of the state X in solution, that is, calculated in the presence of the perturbation caused by the solvent. Ψ_{X} is obtained by solving the effective Schrödinger equation, Eq. (5). E_{B} and E_{A} are calculated using the geometries optimized in solution and do not include the solute–solvent interaction energy.

The ΔG_{int} term is calculated with the free energy perturbation (FEP) method [44], and takes into account the ensemble of thermally accessible solute–solvent configurations. To obtain ΔG_{int}, the solute geometry, charges, and Lennard-Jones parameters are considered as a function of the perturbation parameter λ: when $\lambda = 0$ they correspond to the initial state and when $\lambda = 1$ to the final state. A series of intermediate arbitrary states are defined by linear interpolation of the solute properties and for each of them a fully classical MD simulation is performed. The free energy difference is calculated from these simulations in the usual FEP way. It must be noted that, although geometries and charges for the initial and final states of the solute are calculated quantum mechanically with the ASEP/MD method, the ΔG_{int} term is obtained through classical simulations. This approximation does not introduce significant errors if a sufficiently good solute charge distribution is used and it permits an important saving in computational

effort. A more detailed discussion of this point can be found in Ref. [45]. For a comparison of several strategies based on the MFA for the calculation of solvation free energies in solution and protein environment, see Ref. [46].

Finally, the $\Delta ZPE_{\text{solute}}$ term is calculated in the same way as usually done for in vacuo calculations, using the harmonic approximation for vibrational modes. The only specific consideration in solution is that the molecular geometry and vibrational frequencies of the solute are obtained in solution, using the approximate in solution Hessian matrix. Rotational and translational degrees of freedom are transformed into low-frequency vibrational modes in solution, and must be treated accordingly.

4. VALIDITY OF THE MEAN FIELD APPROXIMATION

The main source of error associated to the use of the MFA is the complete neglect of the Stark component of the solute–solvent interaction energy. In this section, we present some results that permit to estimate the magnitude of this error in several quantities. More specifically, we discuss three types of errors: errors on the energy and dipole moment of molecules in the ground state, errors on the solvent shift in electron transitions, and errors on the energy gradients.

In Table 3.2, the values for the energy and dipole moment of several alcohols and carbonyl compounds in water solution calculated with the MFA or as an average of QM calculations are compared [20]. $\langle A \rangle$ represents the value of the A property calculated as the mean value of 100 quantum calculations; A_{MFA} represents the value obtained when the MFA is used, and has been obtained by calculating the ASEP with the same 100 solvent configurations and performing only one quantum calculation. W_{Stark} is the

Table 3.2 Interaction energy, solvent Stark component (in kcal/mol), and dipole moments (in debyes) in the liquid state calculated as a mean value $\langle E \rangle$ or with the mean field approximation E_{MFA}

	$\langle E \rangle$	E_{MFA}	W_{Stark}	$\langle \mu \rangle$	μ_{MFA}	$\langle \mu \rangle - \mu_{\text{MFA}}$
CASSCF						
Formaldehyde	–9.2	–8.8	0.4 (4.3%)	2.99	2.99	0.00 (0.0%)
Acetaldehyde	–8.9	–8.5	0.4 (4.5%)	3.46	3.46	0.00 (0.0%)
Acetone	–21.9	–21.1	0.8 (3.6 %)	4.48	4.47	0.01 (0.2%)
MP2						
Methanol	–18.3	–17.9	0.4 (2.2%)	2.46	2.45	0.01 (0.4%)
Ethanol	–15.8	–15.4	0.4 (2.5%)	2.27	2.25	0.02 (0.9%)
Propanol	–13.7	–13.5	0.2 (1.5%)	2.15	2.13	0.02 (0.9%)

difference between these two quantities for the energy. As we can see W_{Stark} is in all cases lower than 5% and the errors introduced by the MFA in the dipole moments are lower than 1%. Percentually, the errors are very similar along each series of molecules. The errors are somewhat higher in the carbonyls because of their larger polarizabilities.

For the determination of the error introduced by the MFA in the calculation of the solvent shift of electron transitions, we must compare the transition energy when the MFA is used and when it is not. In Table 3.3, we compared the errors introduced by the MFA in the calculation of the transition energy in several chromophores and different solvents: water, methanol, and cyclohexane. In this study electronic transitions to the first (n–π^*) excited state were studied for acrolein and formaldehyde, whereas (π–π^*) transitions were studied for *p*-difluorobenzene (*p*-DFB) and *trans*-difluoroethene (*trans*-DFE). A practical coincidence is observed between the in solution transition energies obtained using the MFA and those achieved as the average of the transition energies resulting from 100 quantum calculations corresponding to as many solvent configurations. A similar trend can be noted in solvent shift values,

Table 3.3 Transition energies in vacuo, ΔE^0, and in solution calculated as a mean value $\langle \Delta E^d \rangle$ or with the mean field approximation ΔE^d_{MFA}. δ stands for the solvent shift. W_{Starrk} is the solvent Stark component of the solute–solvent interaction energy. All the quantities in kcal/mol

	ΔE^0	$\langle \Delta E^d \rangle$	ΔE^d_{MFA}	$\langle \delta \rangle$	δ_{MFA}	$W_{\text{Stark}}(\delta)$
Water						
Acroleine; CASPT2(6,5)//CASSCF(6,5)	83.08	88.26	88.60	5.18	5.51	0.34
Formaldehyde; CASPT2(4,2)//CASSCF(4,2)	92.30	95.79	95.73	3.49	3.43	–0.06
p-DFB; CASPT2(6,6)//MP2	110.02	111.18	111.17	1.16	1.14	–0.02
trans-DFE; CASPT2(2,2)//MP2	190.62	192.34	189.68	1.72	1.67	–0.05
Methanol						
p-DFB; CASPT2(6,6)//MP2	110.02	110.66	110.75	0.64	0.72	0.08
trans-DFE; CASPT2(2,2)//MP2	190.62	191.60	191.42	0.98	0.80	–0.18
Cyclohexane						
p-DFB; CASPT2(6,6)//MP2	110.02	110.22	110.18	0.16	0.19	–0.03

calculated as the difference of electronic transition energies obtained in vacuo and in solution. Consequently, and as a first conclusion, we can state the absence of solvent Stark effect and the validity of the MFA in the study of the solvent effect on the position of the absorption bands in electronic spectra.

Finally, in Table 3.4 we compare the values of the different components of the free energy gradient for a molecule of formamide in aqueous solution [41]. The error introduced by the MFA in the gradient root mean square (RMS) is close to 1%, very similar to the errors introduced in the energy or in dipole moment. This implies that the MFA can provide good optimized geometries of molecules in solution. In the gradient we have included only the electrostatic component of the solute–solvent interaction energy because the MFA affects only this component, the contribution of the van der Waals component to the gradient is evaluated directly from the MD simulations (vide supra).

Table 3.4 Cartesian gradient of the free energy (in 10^{-3} E_h/a_0) of a molecule of formamide in aqueous solution. Only the electrostatic contribution is included

		Mean of 1000 configurations	Average configuration	Difference
N1	x	12.914	12.827	0.087
	y	3.858	3.831	0.027
	z	0.084	0.085	–0.001
H2	x	–3.365	–3.132	–0.233
	y	3.049	2.928	0.121
	z	0.053	0.049	0.004
H3	x	–1.116	–1.081	–0.035
	y	–5.347	–5.081	–0.266
	z	–0.006	–0.004	–0.002
C4	x	–26.864	–26.816	–0.048
	y	5.473	5.487	–0.014
	z	–0.002	–0.010	0.008
O5	x	18.255	17.862	0.393
	y	–10.052	–9.788	–0.264
	z	–0.041	–0.026	–0.015
H6	x	1.567	1.571	–0.004
	y	–2.136	–2.240	0.104
	z	–0.004	0.002	–0.006
r.m.s.		8.898	8.807	0.091

5. EXAMPLES OF APPLICATIONS

In this section we present some examples of application of ASEP/MD. These examples comprise solvent effects on conformational and configurational equilibria, chemical kinetics, UV/Vis spectra and nonradiative de-excitation of excited states. In all of them, the use of the MFA permits to reduce the computational cost associated to the great number of thermally accessible solvent configurations; this makes it possible to increase the description level of the solute and the use of quantum methods similar to those commonly used in gas-phase calculations: density functional theory (DFT), Møller-Plesset perturbation theory (MP2), complete active space self consistent field (CASSCF), complete active space perturbation theory (CASPT2), and so on. Along this discussion, the results obtained with ASEP/MD will be compared with those obtained with other methods. The final aim is to establish the validity of the MFA and to determine the possible importance of solute–solvent specific interactions on the calculated properties.

5.1. Conformational and configurational equilibria

5.1.1. Anomeric effect in xylopyranose and glucopyranose

The anomeric effect describes the axial preference for an electronegative substituent on the pyranose ring adjacent to the ring oxygen. This effect makes the β-anomer—with all the hydroxyl groups in the equatorial orientation with respect to the ring (in D-glucopyranose)—less stable than the α-anomer—which differs from the β-anomer in the axial orientation of the hydroxyl group on C_1—in vacuo. However, the reverse behavior has been observed in aqueous solution. So, for instance, in D-glucopyranose in water solution, the ratio between α- and β-anomers is 36:64. A similar behavior has been observed in xylopyranose.

In the study of D-xylopyranose [47], the energy and wave functions were calculated using DFT with the Becke three-parameter Lee–Yang–Parr (B3LYP) functional [48] and the 6-311G++G(2d,2p) basis set [49]. For each anomer, there are several possible arrangements of the hydroxyl groups. In general, for the isolated molecule, the hydroxyl groups prefer to orient in such a way as to yield a cooperative hydrogen bonding as efficiently as possible. The two preferred arrangements of the intramolecular hydrogen bonds (IHBs) are clockwise or counterclockwise, the counterclockwise orientation being somewhat more stable. The main results obtained are displayed in Figure 3.3. For comparison, we also give the results obtained with the polarizable continuum model (PCM) [12] as implemented in Gaussian 98 [50] and with a scale factor for the radius of each atomic sphere of 1.2. The continuum model erroneously predicts that solvation favors the α-anomer; in fact, the solvation free energy is 1.1 kcal/mol larger in the α-anomer than in the β. On the contrary, ASEP/MD, which includes specific

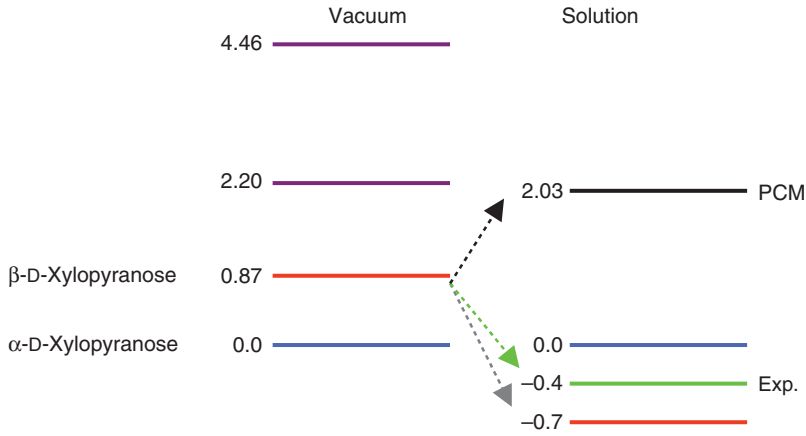

Figure 3.3 Relative free energies (with counterclockwise α-D-xylopyranose as the reference) of α- and β-D-xylopyranose, in vacuo and in solution.

solute–solvent interactions, predicts the correct trend: in solution the more stable form is the β-anomer. Given that in vacuo the anomeric effect favors the α-anomer, the greater stability in solution of the β-anomer must be due to a more favorable solvent interaction term. The relative stability predicted by ASEP/MD, 0.6 kcal/mol, agrees very well with the experimental value, 0.4 kcal/mol [51].

The study of the D-glucopyranose molecule [52] is somewhat more complicated because the hydroxymethyl group can adopt different orientations (see Figure 3.4) with different values of the dihedral angle

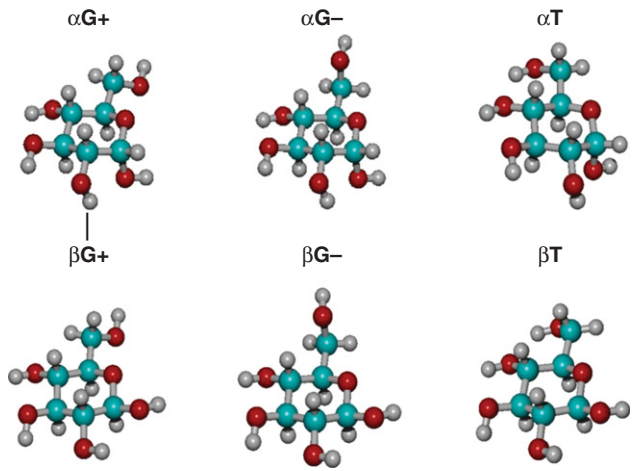

Figure 3.4 Structures of the different rotamers of α- and β-D-glucopyranose.

O_R—C_5—C_6—O_6. In our study we considered the three most important rotamers (T, G+, G–) of counterclockwise D-glucopyranose, which were studied in vacuo and in water solution at the B3LYP/6-31+G(d,p) level and with the ASEP/MD method.

Figure 3.5 shows the relative energies of the six studied conformers of D-glucopyranose in vacuo and in aqueous solution. The energy of the most stable conformer in vacuo, αT, is arbitrarily taken as the reference value. The most significant effect of the solvation of D-glucopyranose is the larger stabilization of the β-conformers relative to the α ones. As a result, we found that while in vacuo the α-conformers are more stable than their β counterparts; in aqueous solution any of the β-conformers is preferred to any of the α-conformers. The difference in energy in solution between the most stable β-conformer, βG+, and the most stable α-conformer, αT, is 0.9 kcal/mol. Experimental evidence [53,54] suggest that the difference in free energy between α- and β-conformers of D-glucopyranose in aqueous solution is around 0.4 kcal/mol (a ratio between α- and β-abundances of 36:64). Our results slightly overestimate these differences in energy (we obtain a ratio between α and β of 20:80), but, given the approximations made in our study, this result is very encouraging.

In order to gain a deeper insight into the solvation effects, in Figure 3.6 we plot the radial distribution function (RDF) for the distances between the anomeric oxygen, O_1, and the water solvent oxygen, O_w, for the six

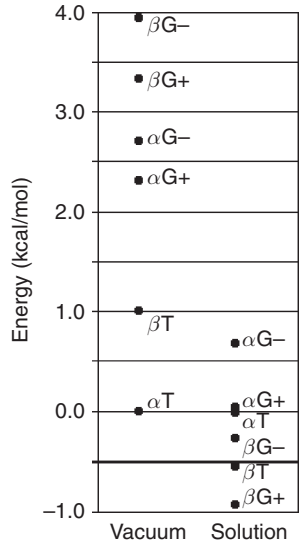

Figure 3.5 Relative free energies (with αT as the reference) of the different rotamers of α- and β-D-glucopyranose, in vacuo and in solution.

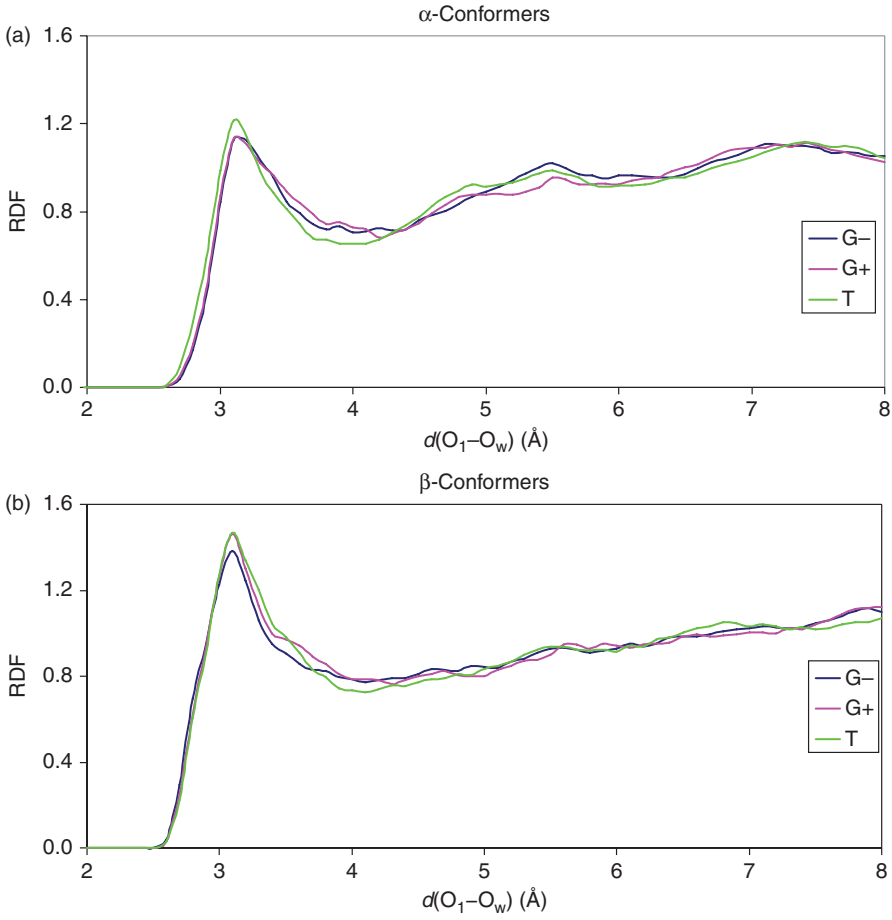

Figure 3.6 O(anomeric)—O(water) RDFs of the different rotamers of α- and β-D-glucopyranose.

conformers. Figure 3.6a shows the RDF for the α conformers and Figure 3.6b for the β-conformers. The main conclusion is that, as we noted above, solvation is more effective for the β-conformers, which shows a peak (at around 3.1 Å) that is higher than for the α-conformers. One can therefore expect the β-conformers to be more stabilized by solvation than the α-conformers, the solvent molecules being more tightly bonded to the anomeric oxygen in the β-conformers. The solvation of the rest of the OH groups of the pyranose ring hardly depends at all on the type of conformer, and hence has no influence on the relative stability of the α- and β-forms.

In sum, the most significant effect of the solvation of D-xylopyranose and D-glucopyranose is the greater stabilization of the β-conformers relative to

the α-conformers. The explanation is that the anomeric effect, which makes α-conformers more stable in the gas phase, is not powerful enough to compete with the effect of a stronger interaction between the solvent and the free electron pairs of the anomeric oxygen in the β-conformers than in the α-conformers, where this interaction is hindered by the rest of the pyranose ring.

5.1.2. Conformational equilibrium in a tripeptide

In recent years, small peptides have been used as model systems for the study of the conformational behavior of more complex biomolecules. In an effort to gain insight on the solvent influence on the structure and stability of peptides, we undertook the study of the electronic structure, the geometric parameters, and the physicochemical properties of the tripeptide Cys-Asn-Ser (Figure 3.7) both in gaseous and in acidic aqueous solutions [55]. The study was performed with ASEP/MD and at the B3LYP/6-311+G (d) level. The Cys-Asn-Ser tripeptide can form several IHBs that involve groups of very different nature [56]. It is hence a good model to check the solvent influence on the geometry and energy of the different groups. We are especially interested in the study of the IHB formed by the oxygen (O25) of the side chain of Asn with the two hydrogens (H2 and H19) bonded to the

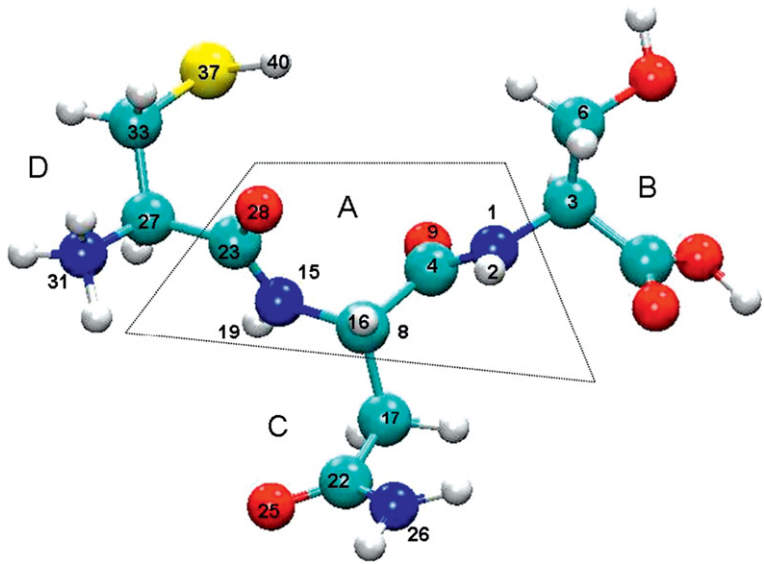

Figure 3.7 Structure and labeling of the Cys-Asn-Ser tripeptide.

nitrogens (N1 and N15) of the peptide bonds, because they can provide stiffness to the main chain of the tripeptide. We named these IHBs as HB1a (N1—H2—O25) and HB1b (N15—H19—O25), respectively.

In gas phase we found three minima, see Figure 3.8. The two more stable structures are Vac-2 and Vac-3, the free energy difference between these two structures is only 0.3 kcal/mol. In both structures, O25 is involved in the formation of an IHB. Somewhat higher in energy (2 kcal/mol), we find Vac-1, in this structure the O25 IHB is missing.

Next, we analyzed the in solution results. Figure 3.9 displays the six more stable structures, for the sake of simplicity other structures at higher energies have not been included. The structures of Sol-1–Sol-3 conformers are equivalent to those obtained in vacuo (Vac-1–Vac-3), in the sense that they are characterized by the same number of IHBs and display a similar orientation of the side groups. Sol-4–Sol-6 are extended structures without IHB. The first conclusion is that the number of local minima is greater in solution than in vacuo. The solvent stabilizes extended structures without IHB that are not stable in vacuo. These results confirm previous studies on the relative stability of amino acids and peptides, where it was found that

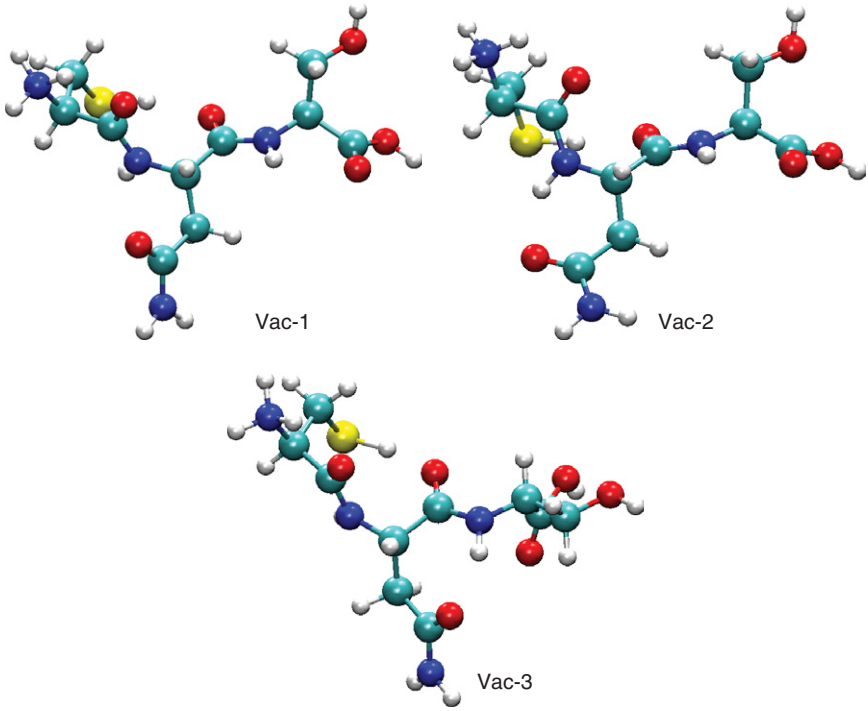

Figure 3.8 Stable conformations of the tripeptide in vacuo.

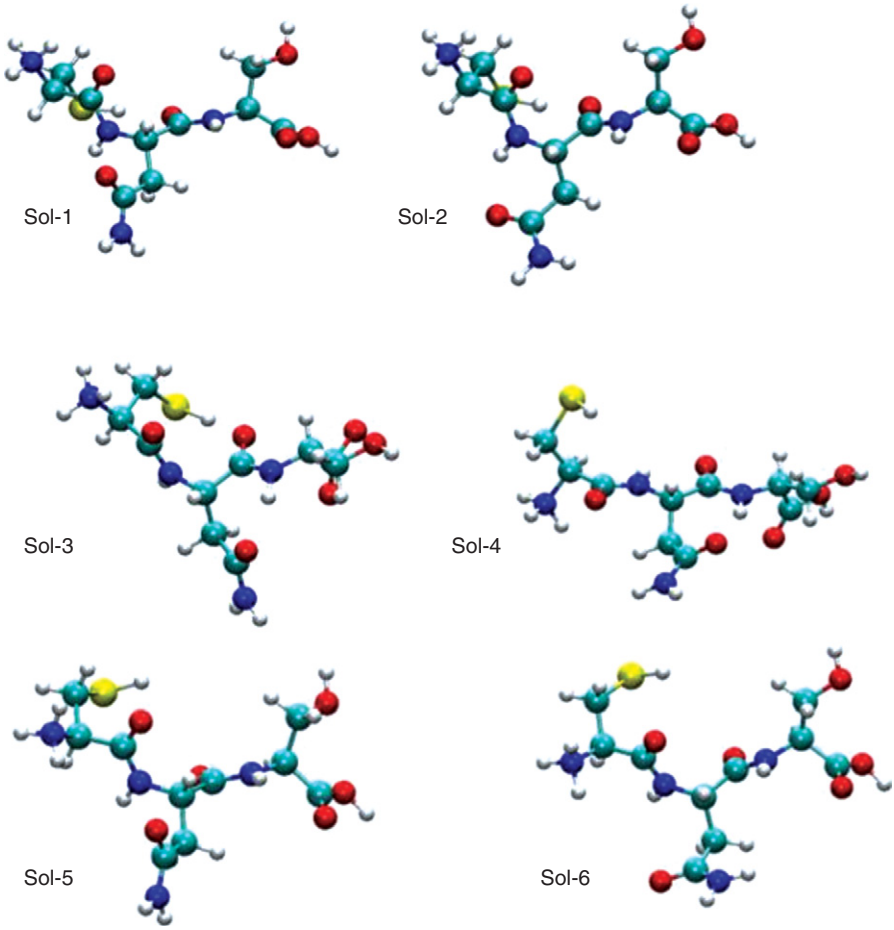

Figure 3.9 Stable conformations of the tripeptide in solution.

some structures that do not exist in gas phase become stable in solution because of their ability to form strong intermolecular HBs with water. So, for instance, in solution, the most stable structures are Sol-1, Sol-5, and Sol-6; in these three conformers, O25 forms an intermolecular HB with the water molecules. Higher in energy are Sol-2 and Sol-3, characterized by the presence of HB1b and HB1a, respectively. Consequently, in solution there is an equilibrium between several structures, with the structures where O25 forms intermolecular HBs strongly favored.

Another fact to emphasize is that, in solution, the stability order is reversed with respect to the situation found in vacuo, here the order is Vac-3 > Vac-2 > Vac-1 whereas in solution the stability order of the equivalent structures is Sol-1 > Sol-2 > Sol-3. The study of the different

Table 3.5 Free energy difference and its components, in kcal/mol, for the six most stable minima found in solution

	ΔE_{solute}	ΔG_{int}	ΔG
Sol-1	–8.0	3.1	–4.9
Sol-2	–11.0	7.4	–3.6
Sol-3	–11.8	9.8	–2.0
Sol-4	0.0	0.0	0.0
Sol-5	4.1	–8.8	–4.7
Sol-6	8.2	–13.0	–4.8

contributions to the free energy, Table 3.5, permits us to clarify the origin of the inversion in the differential stability of the conformers when we pass from gas phase to solution. ΔG is the sum of two contributions: the internal energy, ΔE_{solute}, and the solvation energy, ΔG_{int}, as indicated in Eq. (11) neglecting the ΔZPE_{solute} term. It is interesting to note that there exists a strong negative correlation between the internal energy and the solvation energy: the less stable the internal structure of the conformer, the greater the solvation energy. The internal energy is stabilized by the presence of IHBs, consequently, the most negative values of the internal energy correspond to those structures with the larger number of IHB (Sol-2 and Sol-3). On the contrary, the solvation energy is larger in those structures where there is a better exposure of the polar groups of the peptide to the water molecules, that is, in those structures in which the tripeptide adopts a more extended conformation without IHB (Sol-5 and Sol-6). The stability order results from the interplay of these two factors: internal energy and solvation that, in turn, are determined by the competition between intra- and intermolecular HBs.

The study of the shape of RDF and of the coordination numbers also reveals the competition between IHBs and intermolecular HBs, see Figure 3.10. If one fixes the attention on the O25(tripeptide)—H(water) RDF, it can be noted that the height of the RDF and the coordination number decreases as we pass from a conformation with intermolecular HB to one with intramolecular HB. So, for instance, the O25 coordination number decreases from 2.5 to 2.2 when one passes from Sol-1 to Sol-2, and to 1.8 in Sol-3. However, the most dramatic effects are displayed by H2 and H19. In Sol-1, both hydrogen atoms show well-defined peaks at 2 Å in the H(tripeptide)—O(water) RDFs. In the two cases, the coordination numbers are close to 1. In Sol-2, H2 displays also a very well-defined peak but the RDF associated to H19 has completely lost its structure, evidencing the existence of an IHB between O25 and H19. Something similar is found in Sol-3, in this case the H19—O(water) RDF displays a very well-defined peak but the H2—O(water) RDF loses its structure as a consequence of the H2—O25 IHB.

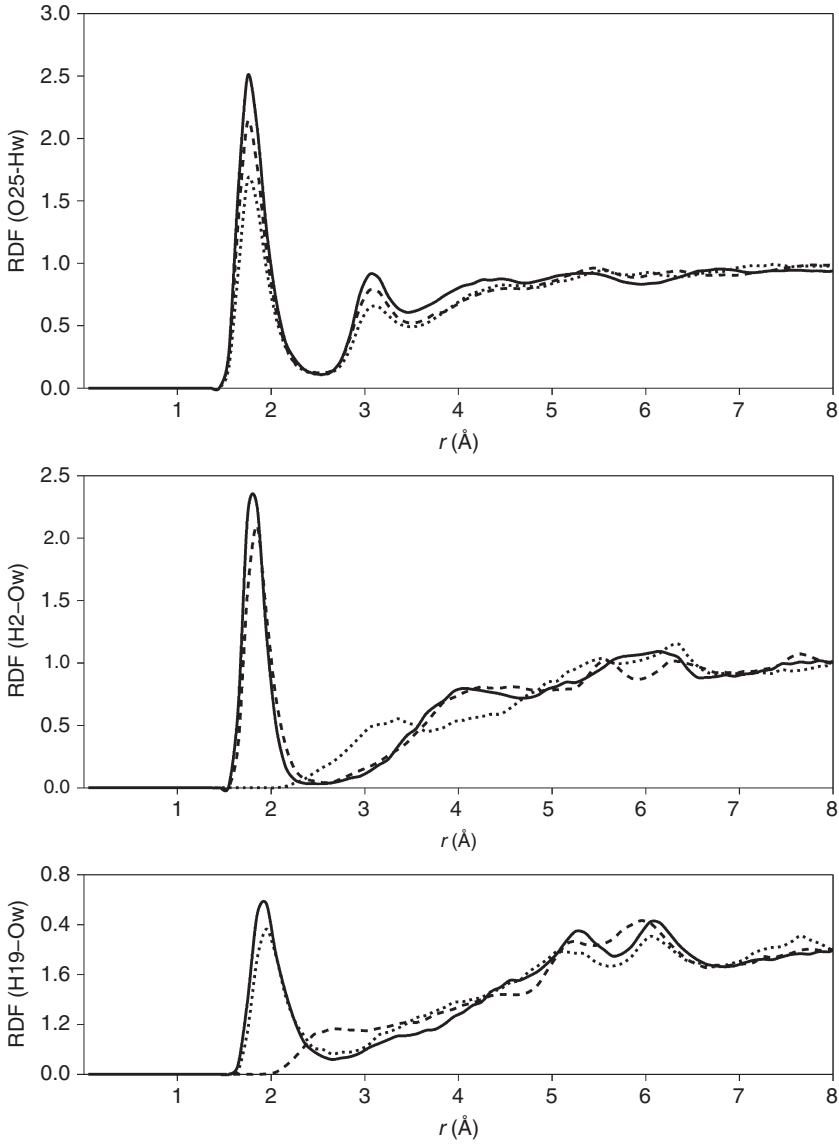

Figure 3.10 O25—H, H2—O, and H19—O RDFs for the tripeptide in solution. Solid: Sol-1. Dashed: Sol-2. Dotted: Sol-3.

5.2. Chemical reactions

An example of application of the ASEP/MD methodology to chemical reactions was the study of the 1,3-proton shift in triazene (N_3H_3) [57]. The ASEP/MD method was used to optimize the geometries of the triazene

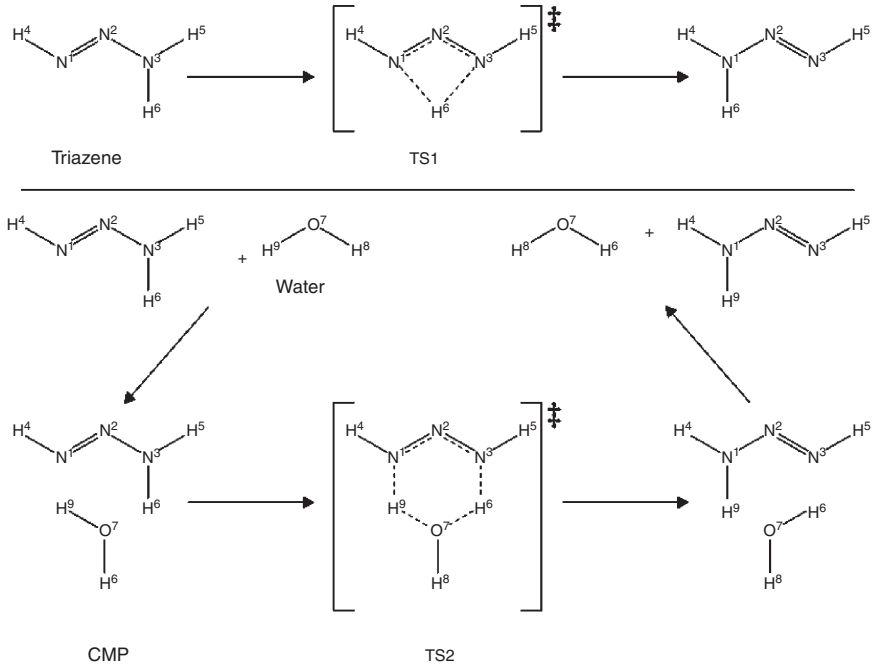

Figure 3.11 Scheme of 1,3 proton shift of triazene. Top: unimolecular reaction. Bottom: bimolecular reaction with the aid of a water molecule.

molecule in water, as well as the transition states of two possible reaction mechanisms: a unimolecular shift (TS1) and a bimolecular reaction aided by a water molecule (TS2, see Figure 3.11) in aqueous solution. A DFT method with a BP86 functional [58,59] was used for the quantum calculations with a triple-zeta basis set. Concerning the structure of the transition states, it was found that TS2 in solution resembles a $N_3H_4^+ + OH^-$ ionic pair in solution more than in gas phase, which accounts for a part of the stabilization of this transition state in solution (see Table 3.6). While the activation energy for the unimolecular reaction increases from 32.0 kcal/mol in gas phase to 34.9 kcal/mol in solution, for the bimolecular reaction it decreases from

Table 3.6 Energy barriers (in kcal/mol) of the two activation processes for the 1,3 proton shift in triazene. See Figure 3.11 for the structures

	In vacuo	In solution
$N_3H_3 \rightarrow$ TS1	32.03	34.91
$N_3H_3 + H_2O \rightarrow$ TS2	10.07	5.46

10.1 kcal/mol to 5.5 kcal/mol. Not only the bimolecular path is preferred, but the preference is much stronger in solution.

As a complementary application, the optimized TS2 structure obtained in water with the ASEP/MD method was used as the initial solute geometry for trajectory calculations with a standard QM/MM method (DFMM) [60–62], using the "rare event" approach for the dynamical study of the bimolecular reaction. Starting with the transition state, 50 different QM/MM trajectories, with Boltzmann-distributed initial velocities, were run both forward and backward in time. This allowed us to observe the behavior of the transition state structure in solution and the course of the reaction. The main conclusions were (1) the hydrogen-bonded complex (CMP) is maintained before and after the reaction takes place; (2) a transition-state-like structure, which resembles an ionic pair, is relatively long-lived (an average life of 85 fs); (3) the calculated transmission coefficient was 0.73, indicative of a good initial representation of the transition state, which was the aim of the ASEP/MD method, and at the same time of a nonnegligible influence of dynamical effects and recrossings, as suggested by the long-lived TS2-like structure.

5.2.1. Electron transitions

In the study of solvent effects on electron spectra, it is very usual to consider two time scales: a fast one, associated with the motion of the electrons, and a slow one, related to the nuclear motion. During an electron transition, the Franck–Condon (FC) principle establishes that the nuclear geometries of the solute and solvent remain fixed. That means that for an absorption process the solvent structure will be in equilibrium with the ground-state solute charge distribution, but not with the solute charge distribution of the excited state (the contrary is valid for the emission process). However, the response of the electron distribution of the solvent is in general fast enough to adapt to the change in the solute charge distribution during the transition. In our group we have developed a polarizable solvent version [63,64] of the ASEP/MD method that permits the electronic degrees of freedom of the solvent to respond instantaneously to the change in the solute charge distribution during the transition, that is, the electron solvent polarization is always in equilibrium with the solute charge distribution. To this end an additional self-consistent process is performed. Using the solvent structure and solute geometry obtained in the first self-consistent ASEP/MD process, we couple the quantum mechanical solute and the electron polarization of the solvent. We assign a molecular polarizability to every solvent molecule, and simultaneously, we replace the effective solvent charge distribution used in the MD simulation with the gas-phase values for the solvent molecule. The induced dipole moment on each solvent molecule is a function of the induced dipole moments on the rest of the molecules and of the solute charge distribution, and hence the electrostatic equation has to be solved

self-consistently. The process finishes when convergence in the solute and solvent charge distributions is achieved.

In our method, the solvatochromic or solvent shift of an electron transition is the sum of several contributions [65] corresponding to the change in the internal energy of the solute when polarized, the distortion energy of the solvent, that is, the energy spent in the reorganization of the solvent during the excitation, and several terms associated to the interactions between the solute charge distribution, Q, and the permanent, q, and induced, p, charges in the solvent.

$$\delta = U_{\text{ex}} - U_{\text{g}} = \frac{1}{2}\delta_{pq} + \delta_{Qq} + \frac{1}{2}\delta_{Qp} + \delta_{\text{dist}}^{\text{solute}} + \delta_{\text{dist}}^{\text{solvent}}. \tag{13}$$

The last term of Eq. (13), the distortion energy of the solvent, vanishes in a vertical transition where the solvent structure is kept fixed but takes a nonnull value in adiabatic transitions.

As an example of application of the method, the transition energy of dimethylaniline (DMA) in several solvents is presented [66]. The geometry of DMA was optimized at CASSCF(8,7)/6-311G** level, and the transition energies calculated with second-order perturbation theory (CASPT2) as implemented in MOLCAS-6 [67]. The solvents, water, cyclohexane, and tetrahydrofuran, were represented as rigid molecules with the OPLS-AA force field. In vacuo, the ground-state dipole moment is 1.33 D and 1.66 D in the excited state. When the molecule is introduced into a solvent, it is expected that the excited state will be more stabilized than the ground state, consequently the transition energy will decrease and we will have a red solvent shift. In Figure 3.12 white circles represent the experimental values. As one can see, the decrease of the transition energy becomes larger when the solvent polarity increases. Water, however, presents an anomalous behavior. In water, the transition energy increases. We will try to explain the reasons of this anomalous behavior later. First, we will describe the prediction of continuum models, blue circles. As we can see, PCM reproduces the experimental trend in nonprotic solvents, but fails in the water case. On the contrary, ASEP/MD, red circles, reproduces correctly the experimental trend, both in protic and nonprotic solvents. The systematic deviation of our results from the experimental values is due to the neglect of the contribution of the dispersion component. This component is a function of the refraction index of the solvent and hence it hardly depends on the solvent nature (the refraction index varies very little among the different solvents studied) and its contribution can be eliminated by considering the differences between solvents instead of the absolute transition energy, see Figure 3.13. The agreement with the experiment is very good.

Turning to the motives of the anomalous behavior of water, in Figure 3.14 we represent the occupancy map of water oxygen atoms. Because of the formation of HBs, most of the water molecules concentrate close to the free

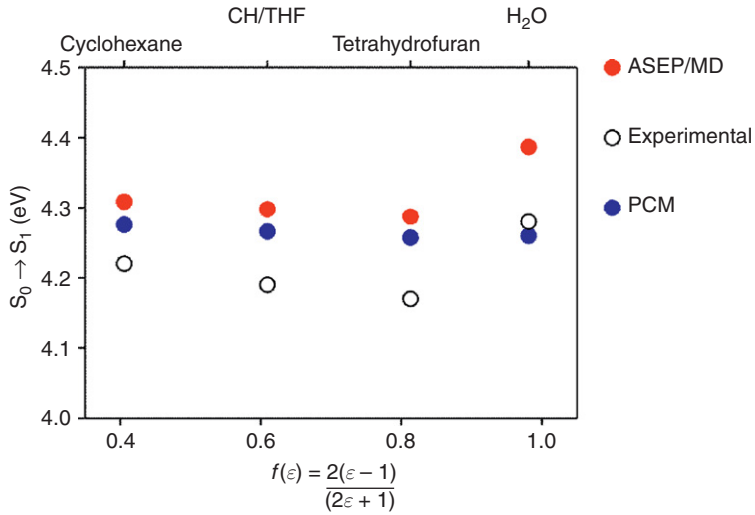

Figure 3.12 Absorption energies of DMA in solvents of different polarity.

electron pair of the nitrogen atom. There are also high concentrations above and below the aromatic ring. When the molecule is excited, part of the charge is transferred from the nitrogen atom to the ring, and the HBs are broken, as a consequence the solvation energy decreases in the excited state. In reality, this is only a partial view of the problem. When the solute molecule is placed in

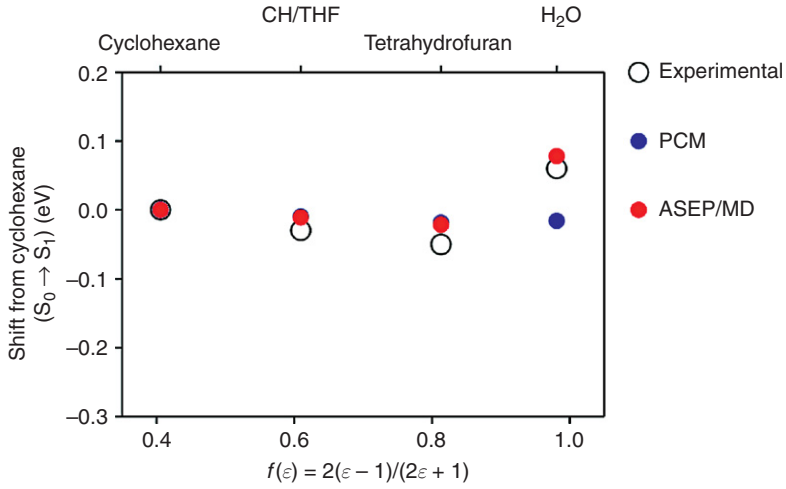

Figure 3.13 Relative absorption energies of DMA in solvents of different polarity, with cyclohexane as the reference.

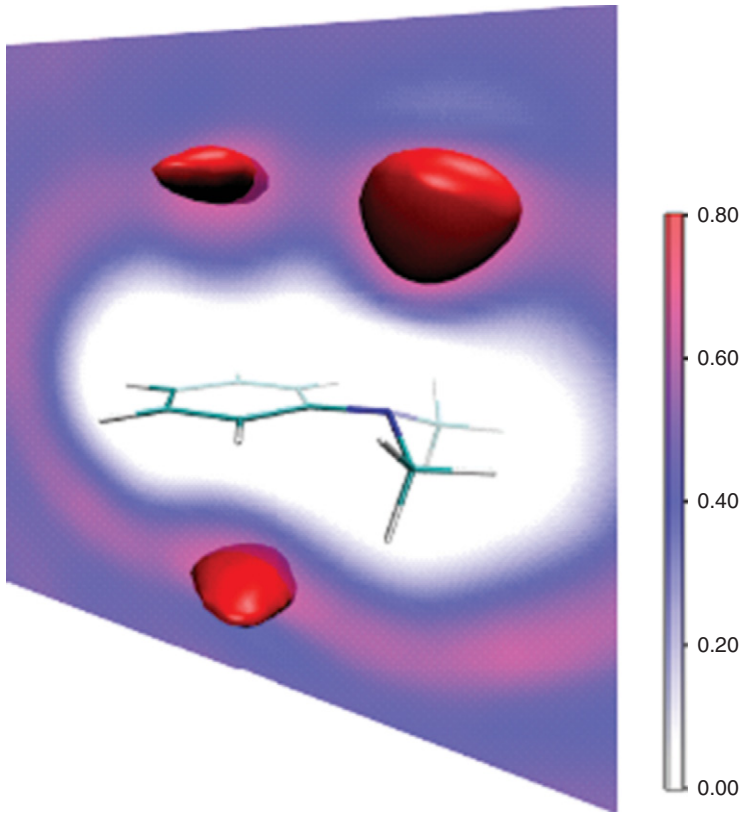

Figure 3.14 Occupancy map of oxygen atoms around the ground state of DMA. Solid isosurface at a density value of 0.64.

water, the wagging angle between the dimethylamino and phenyl moieties increases, see Table 3.7, something that does not occur with the other solvents. Almost half of the solvent shift comes from this distortion of the geometry, the rest is explained by the breaking of the HBs mentioned before.

Table 3.7 Twisting angle (in degrees) for optimized geometries of DMA in several solvents

	Angle
Gas	28.4
Cyclohexane	28.7
CH/THF (0.5)	28.5
Tetrahydrofuran	28.5
Water	34.0

Another interesting case is the study of the solvent effects on the electron transitions in retinal [68,69]. Retinal is a very interesting molecule because it is the chromophore of rhodopsin, the visual pigment in vertebrates. The (π–π^*) electron transitions to the first two excited states of 11-*cis*-retinal protonated Schiff base (PSB) and several simplified models that have been profusely used in the bibliography (see Figure 3.15) were calculated in vacuo and in methanol solutions. The ASEP/MD method was employed for the in solution calculations. Full ground-state geometry optimizations were performed in both conditions, allowing the total relaxation of all the degrees of freedom at MP2 and/or CASSCF level of calculation with the split-valence 6-31G* basis set. Nevertheless, the transition energies were always obtained at CASSCF/6-31G* level of calculation using in each case the complete active π space (10e, 10o), or (12e, 12o) depending on the model used. To improve the energy results, the dynamic electron correlation energy was included with second-order perturbation theory (CASPT2).

In vacuo, the first transition gives rise to a very strong band, while the transition to the second state is almost forbidden. In the ground and second excited states, the positive charge is localized close to the nitrogen atom (covalent states); however, in the first excited state the charge is spread out on the entire molecule (ionic state), see Figure 3.16. Consequently, the second excited state will solvate better than the first and one expects that the energy gap between the two states decreases. In fact, we find that in methanol solution, both states become almost degenerate. Furthermore, the oscillator strength of the transition to the second state increases. This behavior agrees with the experimental spectra [70–72], where, in gas-phase conditions two bands are found, one weak and the other strong but only a single very broad band appears in methanol solution.

Table 3.8 collects vertical transition energies in solution and the corresponding solvent shifts obtained for different models of retinal. At first sight, the interaction with the solvent seems to produce the inversion in the relative position of the first two excited states, the covalent state becoming lower in energy with respect to the ionic one. The nature of the different states was corroborated by the dominant configuration participating in each state, that is, doubly excited for the covalent and a highest occupied molecular orbital (HOMO)–lowest unoccupied molecular orbital (LUMO) transition for the ionic. Oscillator strengths were also calculated, being the transition to the upper excited state the optically allowed transition (f value close to 1). The energy difference between the covalent and ionic states varies between 0.7 eV and 0.3 eV at CASSCF//MP2 level of calculation. The scene changes substantially when dynamic correlation is taken into account. Under these conditions, both states become practically degenerate, and we find an energy gap between them of about 0.1 eV. The proximity between these electron transitions gives rise to the fact that, contrary to the in vacuo conditions, the in solution theoretical absorption spectrum shows

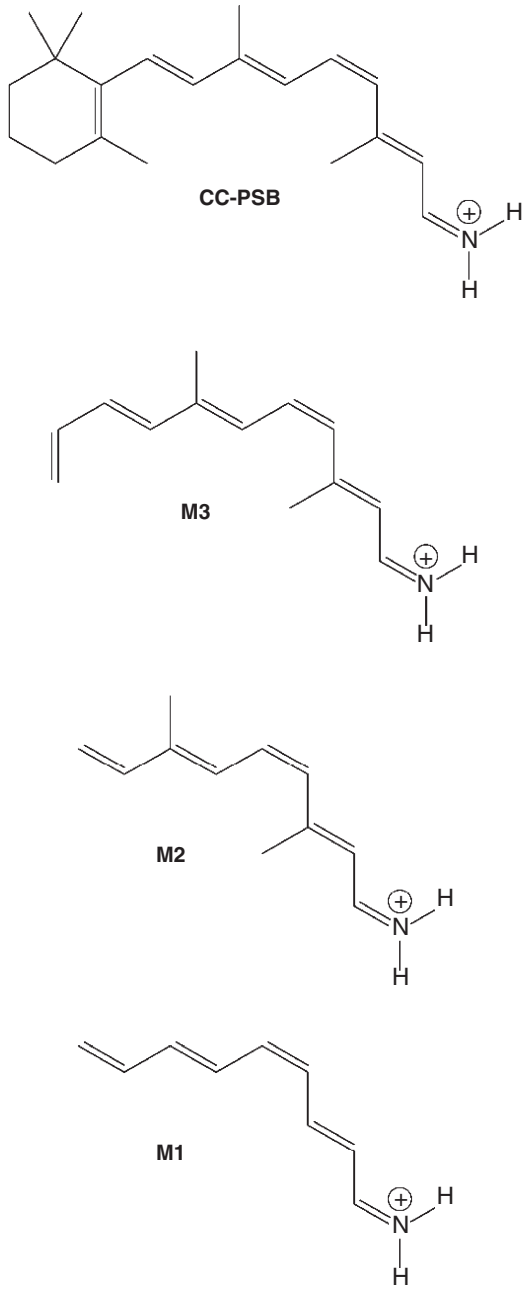

Figure 3.15 Structures of the 11-*cis*-retinal protonated Schiff Base (CC-PSB), and their models used in the study.

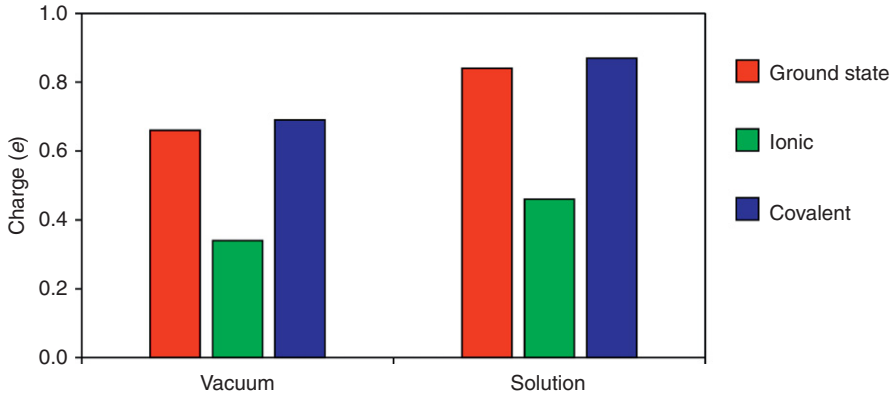

Figure 3.16 Localization of the molecular charge on the iminium half of the retinal molecule (M1 model) in vacuo and in solution, for the three lower electronic states.

Table 3.8 Calculated vertical transition energies (eV), oscillator strengths, and solvent shifts values (eV) for the M1, M2, M3, and CC-PSB models

	$S_0 \rightarrow$Ionic			$S_0 \rightarrow$Covalent	
	Vacuo	Solution	δ	Vacuo	Solution
M1					
CASSCF/CASSCF	3.55	5.22	1.67	4.61	4.62
CASPT2/CASSCF	2.56	3.82	1.26	3.58	3.78
CASPT2/MP2	2.40	3.51	1.11	3.16	3.61
Oscillator strength	1.15	1.00		0.09	0.01
M2					
CASSCF/CASSCF	3.34	4.93	1.59	4.34	4.44
CASPT2/CASSCF	2.56	3.68	1.12	3.64	3.45
Oscillator strength	0.97	0.87		0.21	0.23
M3					
CASSCF/MP2	3.03	4.08	1.05	4.05	3.78
CASPT2/MP2	2.28	2.99	0.71	3.27	2.88
Oscillator strength	0.95	0.91		0.22	0.21
CC-PSB					
CASSCF/MP2	2.54	4.19	1.65	3.42	3.87
CASPT2/MP2	1.93	3.00	1.07	2.77	2.95
Oscillator strength	1.20	0.93		0.06	0.15
Experimental	2.03	2.79		3.18	

two poorly resolved bands. Our results confirm the recent experimental study published by Nielsen et al. [72]. In this study, the authors provide the in vacuo and the in solution electronic absorption spectra of the all-*trans n*-butyl PSB in methanol solution and also the in vacuo spectrum for the 11-*cis* dimethyl Schiff base. The in solution registered spectra for the two isomers are said to be identical. The experimental gas-phase spectrum shows a band at 390 nm corresponding to the S_2 absorption band maximum and another at 610 nm corresponding to the transition to the S_1 state. When the spectrum is recorded in methanol solution, the S_1 band maximum is blue-shifted by more than 150 nm and what is more important, no resolved S_1 and S_2 bands were found. The spectrum shows only a broad band centered at around 450 nm (2.76 eV). Independently of the model used in the calculations, our theoretical results completely reproduce the appearance of the experimental spectra.

Another interesting quantity to evaluate is the predicted solvent shift. These values are also collected in Table 3.8 and were calculated as the shift suffered by the ionic band as a consequence of the solvent effect. Surprisingly, CASPT2 calculations supply practically the same solvent shift (around 1.1 eV) value independently of the system complexity, except for the M3 model where the value is slightly lower. In all cases the calculated value is larger than the experimental one, estimated in 0.72 eV (2.76 eV, the electronic transition energy in methanol solution, minus 2.03 eV, in vacuo). The fact that the complete chromophore (CC)-PSB system shows the same solvent shift overestimation as most simplified models (M1 or M2) is due to a structural characteristic of the system shared by all of them. Most of the solvation energy comes from the interaction between the iminium group and the methanol molecules. In all the systems here considered, the N atom is bonded to two hydrogen atoms; however, the experiments have been performed with molecules where the N is bonded to methyl or bulkier groups. In order to get more details, new calculations were performed. In particular a new model (M4) was built replacing the hydrogen atoms linked to the N atom in M1 with two methyl groups. Both CASSCF and MP2 geometry optimizations were performed in vacuo and in methanol solution keeping the same conditions as in previous calculations. The solvent shift obtained for this model was 0.84 eV and 0.64 eV at CASPT2//CASSCF and CASPT2//MP2 level of calculation, respectively. Comparison with the equivalent results for M1 shows that the methyl groups' incorporation decreases the solvent shift value in around 0.45 eV. If this decrease is directly applied to the CC-PSB solvent shift, the final value becomes 0.65 eV, in very good agreement with experimental data (0.72 eV).

5.3. Nonradiative de-excitations in retinal

Even if the very first step of the visual process can be considered the light-induced promotion of one electron from a π-type orbital to a π^* one in the chromophore of the protein rhodopsin, its biological activity starts with the

cis–trans isomerization that this chromophore suffers in the excited state. This conformational inversion causes in turn a conformational change in the protein and starts the rest of the reactions taking place in the visual process. Inside the protein pocket, this isomerization step is very fast, taking only 200 fs, and no significant fluorescence is usually observed. These properties are characteristic of nonradiative processes involving crossings between potential energy surfaces. These crossings can take place through CIs or singlet–triplet crossings (STC) depending on the identical of different spin symmetry of the involved states, respectively.

In the last decade, there have been quite exhaustive studies on the isomerization of the rhodopsin chromophore through a CI between its covalent ground state and the ionic first excited state in vacuo conditions. Different models for the chromophore representation and more and more accurate methods have been used in these studies. It has been only in the last years when the development of the computational resources has permitted the study of this process in a more realistic way, that is, considering the possible effect of the environment. In our case, we have used an extended version of the ASEP/MD method that allows the location of CIs and STCs of systems in solution. The algorithm implemented in the method is due to Bearpark et al. [73] and simultaneously minimizes the in solution energy difference between the two intersecting states and the energy of the crossing seam between the two potential energy surfaces. See Ref. [74] for more details.

We started our study with the location of the in vacuo minimum energy conical intersection (MECI) structure for the simplest model used in the previous study devoted to the solvent effect on the UV absorption spectrum. The main structural characteristic of this CI is a twist of ∼90° showed by the central original double bond. In order to permit this change in the dihedral angle, it is necessary the inversion in the nature of the single and double bonds with respect to the FC structure, which is clearly observed in Table 3.9. Next, our objective was the study of the solvent influence (methanol, in particular) on the structure and position of the MECI. In this point, two strategies were followed depending on whether the solvent is considered as a frozen solvent or it is allowed to equilibrate with the solute electronic distribution. The first corresponds to an infinitely slow solvent response and the second to an infinitely fast solvent reorganization.

In the equilibrium case, it is possible to locate the MECI in solution, and from a structural viewpoint, the solvent modifies bond distances and slightly the twist of the dihedral angle. What is worth noting is that the solvent suffers an important restructuring around the solute molecule to respond to the torsion of almost 90° of its central dihedral angle from the FC structure. Figure 3.17 displays the occupancy maps of methanol oxygen atoms around the FC and MECI structures. As it can be seen, at the FC point the solvent is mainly concentrated around the iminium end, where the

Table 3.9 Optimized geometries of a retinal model at the Franck–Condon point and at the conical intersection. Bond lengths in ångström, angles in degrees

	FC		MECI S_0/S_1	
	Vacuo	Methanol	Vacuo	Methanol
C_1C_2	1.35	1.34	1.36	1.36
C_2C_3	1.46	1.47	1.42	1.40
C_3C_4	1.35	1.36	1.41	1.41
C_4C_5	1.45	1.45	1.38	1.36
C_5C_6	1.36	1.36	1.47	1.46
C_6C_7	1.45	1.46	1.37	1.41
C_7C_8	1.35	1.36	1.42	1.39
C_8C_9	1.44	1.43	1.39	1.44
C9═N	1.28	1.28	1.32	1.30
Dihedral	Planar	Planar	91.0	85.9

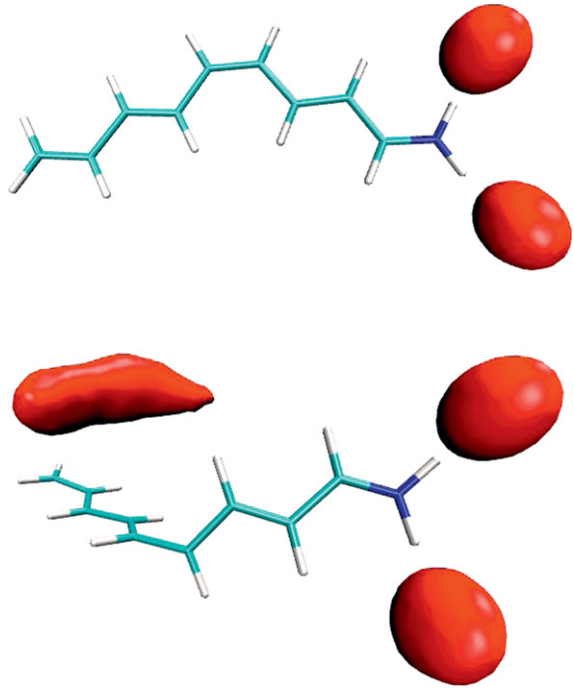

Figure 3.17 Maximum occupancy regions of oxygen atoms around the ground state (top) and the MECI (bottom) of the M1 retinal model.

molecular charge is predominantly located, as at the FC the solvent is in equilibrium with the ground state covalent electronic distribution. At the MECI, one finds solvent molecules around the iminium end but also around the carbon skeleton along which at the excited state the charge is spread out. It can be concluded that in the equilibrium situation solvent molecules stabilize the delocalization of the charge in the excited state and the two states involved in the CI can cross. In frozen solvent conditions, the location of the MECI has been impossible. If the solvation shells are considered fixed and in equilibrium with the ground-state electronic distribution, when the central dihedral angle rotates, part of the solute molecule will overlap with the solvent. In addition, if the solvent can in some way equilibrate with the solute, the great restructuring that it should suffer must take several picoseconds and the isomerization in solution should be slower than in vacuo or inside the protein pocket. This fact agrees with somewhat more persistent fluorescence found for the rhodopsin chromophore in methanol solution [75].

6. SUMMARY

The theoretical study of solvent effects is, in general, very demanding because it requires extensive sampling of the configurational space of the solute–solvent system. The MFA provides a practical and effective approach that opens the possibility of studying chemical equilibria, spectroscopic transitions, kinetic problems, and so on, using computational levels similar to those used for gas-phase systems. The study of different systems and processes in solution has permitted us to conclude that the MFA works very well, even in those cases where the solvent is represented in a simplified way, a dielectric for instance. Obviously, in this case, we must restrict ourselves to systems where specific solute–solvent interactions are not present. If these interactions are present, it is compulsory the use of more sophisticated solvent descriptions that allow accounting for the effect of bulk and specific interactions. ASEP/MD is a method that permits to combine a high-level quantum mechanical description of the solute with a detailed, microscopic, description of the solvent.

The following are the main characteristics of ASEP/MD: (1) A reduced number of quantum calculations that permits to increase the description level of the solute molecule which, in fact, can be described at the same level as in isolated conditions. (2) Since the solvent is described through MM force fields, there exists a great flexibility to include both bulk and specific interactions into the calculations. (3) At the end of the procedure, the solute wave function and the solvent structure become mutually equilibrated, that is, the solute is polarized by the solvent and the solvent structure is in equilibrium with the polarized solute charge distribution. (4) Finally, the

method permits to find in an efficient way the geometry of critical points. With critical points we refer to minima, transition states, CIs, and so on.

In the last section of this chapter, we have presented an overview of applications of the ASEP/MD method to different systems and phenomena. The approximations and methodology used have been validated through comparisons with other studies and accepted methods and, in general, it has been shown that ASEP/MD is a powerful and efficient method that does not introduce significant errors but, in contrast, makes it possible to consistently introduce the solvent influence on high-level quantum calculations. Conformational equilibria, chemical reactivity, and electron transitions are just three areas where solvent effects play an important role and where ASEP/MD has proved to be a valuable tool.

REFERENCES

[1] C. Reichardt, Org. Process Res. Dev. 11 (2007) 105.
[2] S. Canuto (Ed.), Solvation Effects on Molecules and Biomolecules. Computational Methods and Applications, Springer, Berlin, 2008.
[3] M. Born, Z. Phys. 1 (1920) 45.
[4] G.J. Kirkwood, J. Chem. Phys. 2 (1934) 351.
[5] L. Onsager, J. Am. Chem. Soc. 58 (1936) 1486.
[6] C. Reichardt, Solvent and Solvent effects in Organic Chemistry, third ed., Wiley-VHC, Weinheim, 2003.
[7] O. Tapia, in: Z.B. Maksic (Ed.), Theoretical Treatment of Large Molecules and Their Interactions, vol. 4, Springer-Verlag, Berlin, 1991, p. 435.
[8] J.G. Angyán, J. Math. Chem. 10 (1992) 93.
[9] R. Car, M. Parrinello, Phys. Rev. Lett. 55 (1985) 2471.
[10] A. Warshel, M. Levitt, J. Mol. Biol. 103 (1976) 227.
[11] S. Humbel, S. Sieber, K. Morokuma, J. Chem. Phys. 105 (1996) 1959.
[12] J. Tomasi, M. Persico, Chem. Rev. 94 (1994) 2027.
[13] J.L. Rivail, D. Rinaldi, in: J. Leszczynski (Ed.), Computational Chemistry: Review of Current Trends, World Scientific Publishing, Singapore, 1995.
[14] C.J. Cramer, G.D. Truhlar, in: K.B. Lipkowitz, D.B. Boyd (Eds.), Reviews in Computational Chemistry, vol. VI, VCH Publishers, New York, 1995, p. 1.
[15] S. Ten-no, F. Hirata, S. Kato, Chem. Phys. Lett. 214 (1993) 391.
[16] H. Sato, F. Hirata, S. Kato, J. Chem. Phys. 105 (1996) 1546.
[17] F. Hirata (Ed.), Molecular Theory of Solvation (Understanding Chemical Reactivity), Springer, Berlin, 2003.
[18] M.L. Sánchez, M.A. Aguilar, F.J. Olivares del Valle, J. Comput. Chem. 18 (1997) 313.
[19] M.L. Sánchez, M.E. Martín, M.A. Aguilar, F.J. Olivares del Valle, J. Comput. Chem. 21 (2000) 705.
[20] M.L. Sánchez, M.E. Martín, I. Fdez. Galván, F.J. Olivares del Valle, M.A. Aguilar, J. Phys. Chem. B 106 (2002) 4813.
[21] I. Fdez. Galván, M.L. Sánchez, M.E. Martín, F.J. Olivares del Valle, M.A. Aguilar, Comput. Phys. Commun. 155 (2003) 244.
[22] K.V. Mikkelsen, H. Agren, H.J.A. Jensen, T. Helgaker, J. Chem. Phys. 89 (1988) 3086.
[23] K.V. Mikkelsen, A. Cesar, H. Agren, A.J.H. Jensen, J. Chem. Phys. 103 (1995) 9010.
[24] J. Tomasi, B. Mennuci, R. Cammi, Chem. Rev. 105 (2005) 2999.

[25] A. Klamt, G. Shüürmann, J. Chem. Soc., Perkin Trans. 2 (1993) 799.
[26] T.N. Truong, V.E. Stefanovich, Chem. Phys. Lett. 240 (1995) 253.
[27] A. Warshel, Computer Modelling of Chemical Reactions in Enzymes and Solutions, Wiley, New York, 1991.
[28] H. Hu, Z. Lu, J. Yang, J. Chem. Theory Comput. 3 (2007) 390.
[29] H. Hu, Z. Lu, J.M. Parks, S.K. Burger, J. Yang, J. Chem. Phys. 128 (2008) 034105.
[30] H.C. Georg, K. Coutinho, S. Canuto, Chem. Phys. Lett. 429 (2006) 119.
[31] B. Linder, Adv. Chem. Phys. 12 (1967) 225.
[32] G. Karlström, B. Halle, J. Chem. Phys. 99 (1993) 8056.
[33] N. Ghoneim, P. Suppan, Spectrochim Acta, 51 (1995) 1043.
[34] T. Yamamoto, J. Chem. Phys. 129 (2008) 244104.
[35] K. Coutinho, R. Rivelino, H.C. Georg, S. Canuto, in: S. Canuto (Ed.), Solvation Effects on Molecules and Biomolecules. Computational Methods and Applications, Springer, Berlin, 2008, p. 159.
[36] K. Coutinho, H.C. Georg, T.L. Fonseca, V. Ludwig, S. Canuto, Chem. Phys. Lett. 437 (2007) 148.
[37] N. Okuyama-Yoshida, M. Nagaoka, T. Yamabe, Int. J. Quantum Chem. 70 (1998) 95.
[38] N. Okuyama-Yoshida, K. Kataoka, M. Nagaoka, T. Yamabe, J. Chem. Phys. 113 (2000) 3519.
[39] H. Hirao, Y. Nagae, M. Nagaoka, Chem. Phys. Lett. 348 (2001) 350.
[40] Y. Zhang, H. Liu, W. Yang, J. Chem. Phys. 112 (2000) 3483.
[41] I. Fdez. Galván, M.L. Sánchez, M.E. Martín, F.J. Olivares del Valle, M.A. Aguilar, J. Chem. Phys. 118 (2003) 255.
[42] I. Fdez. Galván, M.E. Martín, M.A. Aguilar, J. Comput. Chem. 25 (2004) 1227.
[43] L.W. Jorgensen, Acc. Chem. Res. 22 (1989) 184.
[44] W.R. Zwanzig, J. Chem. Phys. 22 (1954) 1420.
[45] I. Fdez. Galván, M.E. Martín, M.A. Aguilar, J. Chem. Phys. 124 (2006) 214504.
[46] E. Rosta, M. Haranczyk, Z.T. Chu, A. Warshel, J. Phys. Chem. B 112 (2008) 5680.
[47] I. Fdez. Galván, F.J. Olivares del Valle, M.E. Martín, M.A. Aguilar, Theor. Chem. Acc. 111 (2004) 96.
[48] D.A. Becke, J. Chem. Phys. 98 (1993) 5648.
[49] R. Krishnan, J.S. Binkley, R. Seeger, A.J. Pople, J. Chem. Phys. 72 (1980) 650.
[50] J.M. Frisch, G.W. Trucks, H.B. Schlegel, G.E. Scuseria, M.A. Robb, J.R. Cheeseman, et al., Gaussian 98, Gaussian, Pittsburgh, PA, 1998.
[51] C. Höög, G. Widmalm, J. Phys. Chem. B 105 (2001) 6375.
[52] J.C. Corchado, M.L. Sánchez, M.A. Aguilar, J. Am. Chem. Soc. 126 (2004) 7311.
[53] J.S. Angyal, Aust. J. Chem. 21 (1968) 2737.
[54] J.S. Angyal, Angew. Chem. 81 (1969) 172.
[55] C. Soriano-Correa, F.J. Olivares del Valle, A. Muñoz-Losa, I. Fdez. Galván, M.E. Martín, M.A. Aguilar (2010) to be published.
[56] C. Soriano-Correa, J.F. Sánchez-Ruiz, G. Rico-Rosillo, J.A. Giménez-Scherer, J. Velázquez-Rodríguez, R. Kretschmer-Schmid, J. Mol. Struct. (Theochem) 769 (2006) 91.
[57] I. Fdez. Galván, M.A. Aguilar, M.F. Ruiz-López, J. Phys. Chem. B 109 (2005) 23024.
[58] P.J. Perdew, Phys. Rev. B 33 (1986) 8822.
[59] D.A. Becke, Phys. Rev. A 38 (1988) 3098.
[60] I. Tuñón, M.T.C. Martins-Costa, C. Millot, M.F. Ruiz-López, J. Mol. Mod. 1 (1995) 196.
[61] I. Tuñón, M.T.C. Martins-Costa, C. Millot, M.F. Ruiz-López, L.J. Rivail, J. Comput. Chem. 17 (1996) 19.
[62] I. Tuñón, M.T.C. Martins-Costa, C. Millot, M.F. Ruiz-López, J. Chem. Phys. 106 (1997) 3633.
[63] M.E. Martín, M.L. Sánchez, F.J. Olivares del Valle, M.A. Aguilar, J. Chem. Phys. 113 (2000) 6308.
[64] M.E. Martín, M.L. Sánchez, M.A. Aguilar, F.J. Olivares del Valle, J. Mol. Struct. (Theochem) 537 (2001) 213.
[65] M.E. Martín, A. Muñoz-Losa, I. Fdez. Galván, M.A. Aguilar, J. Chem. Phys. 121 (2004) 3710.

[66] I. Fdez. Galván, M.E. Martín, A. Muñoz-Losa, M.A. Aguilar, J. Chem. Theory Comput. 5 (2009) 341.
[67] G. Karlström, R. Lindh, P.-Å. Malmqvist, B.O. Roos, U. Ryde, V. Veryazov, et al., Comput. Mater. Sci. 28 (2003) 222.
[68] A. Muñoz-Losa, I. Fdez. Galván, E. Martín, M.A. Aguilar, J. Phys. Chem. B 110 (2006) 18064.
[69] A. Muñoz-Losa, I. Fdez. Galván, M.A. Aguilar, E. Martín, J. Phys. Chem. B 112 (2008) 8815.
[70] K.A. Freedman, S.R. Becker, J. Am. Chem. Soc. 108 (1986) 1245.
[71] L.H. Andersen, I.B. Nielsen, M.B. Kristensen, M.O.A. El Ghazaly, S. Haacke, M.B. Nielsen, Å.M. Petersen, J. Am. Chem. Soc. 127 (2005) 12347.
[72] I.B. Nielsen, L. Lammich, H.L. Andersen, Phys. Rev. Lett. 96 (2006) 018304.
[73] M.J. Bearpark, M.A. Robb, B.H. Schlegel, Chem. Phys. Lett. 223 (1994) 269.
[74] A. Muñoz-Losa, I. Fdez. Galván, M.L. Sánchez, E. Martín, M.A. Aguilar, J. Phys. Chem. B 112 (2008) 877.
[75] H. Kandori, Y. Katsuta, M. Ito, H. Sasabe, J. Am. Chem. Soc. 117 (1995) 2669.